Proceedings of the XII International Symposium on Dynamic Problems of Mechanics (DINAME 2007),
Varoto, P. S. and Trindade, M. A. (Editors), ABCM, Ilhabela, SP, Brazil, February 26 - March 2, 2007

Modeling and Analysis of a Dynamically Tuned Gyroscope

Ettore Apolônio de Barros [1], Fábio Doro Zanoni[1], Fernando de Castro Junqueira [2]

[1] University of São Paulo. Department of Mechatronics Engineering and Mechanical Systems. Av Prof Mello Moraes, 2231, Cidade Universitária, CEP 05508-900 – São Paulo, SP. Tel. (11)3091-5761. e-mail: eabarros@usp.br.

[2] University of São Paulo. Department of Mechatronics Engineering and Mechanical Systems. Av Prof Mello Moraes, 2231, Cidade Universitária, CEP 05508-900 – São Paulo, SP. Tel. (11)3817-7620. e-mail: fcjunq@usp.br.

Abstract: This work describes the principle of operation and the motion dynamics of a dynamically tuned gyroscope, DTG, in open and closed loop. The complete set of non-linear equations of motion are presented, and a simplified representation for the transfer functions are obtained, emphasizing the concepts related to important parameters, and phenomena that affect the DTG performance. Linear and nonlinear models are compared through simulation of rotor responses to the case motions. A clearer and improved approach to the DTG model is proposed when compared to the classical derivations of Craig (1972 a, b). The work also includes a presentation of the control system electronics, giving a description of each block..

Keywords: *Gyroscope, Inertial Navigation System, Sensor, DTG.*

1.INTRODUCTION.

Inertial sensors (gyroscopes and accelerometers) are an important component for a number of civilian and military applications. Robotics, autonomous vehicles, airplanes, ships, satellites and offshore platforms are some examples of civil use. One also can mention the stabilization of weapons and radars, missiles and torpedoes as military examples. These applications make us to realize the importance for many countries of having their own development of inertial technology.

Particularly, gyroscopes usually involve high cost manufacturing processes, sophisticated technology and expertise, so that the necessary performance on vehicle navigation or device positioning can be achieved. A dynamic tuned gyroscope, the so-called DTG, is one of the options nowadays that can provide the required performance for many applications at a reasonable price. They demand considerable less investment in materials, machinery, processes and man power when compared to the other usual sensors such as the floated or ring-laser gyroscopes.

This work discusses the development of a DTG, emphasizing aspects of modeling the DTG dynamics, and the control system design. Fundamentals and mathematical modeling of a single-gimbaled DTG are introduced at next section. Section 3 presents the derivation of open loop linear model, emphasizing the dynamics of rotor precession and nutation. Section 4 presents the derivation of the precession equations for an ideal DTG. In the section 5, the mistuning effect in DTG operation is analyzed. Section 6 introduces the main characteristics of the DTG control system. Finally, main conclusions and future steps for investigation in the sensor development are discussed in section 7.

2. MATHEMATICAL MODELING OF THE GYROSCOPE DYNAMICS

The DTG operation principle is based on an inertia rotor suspended by a universal joint with flexure pivots (Fig. 1). The flexure spring stiffness is independent of spin rate. However, the dynamic inertia, i.e. the gyroscopic reaction effect from the gimbal, provides negative spring stiffness proportional to the square of the spin speed (Howe and Savet, 1964; Lawrence, 1998). Therefore, at a particular speed, called the tuning speed, the two moments cancel each other, freeing the rotor from torque, a necessary condition for an ideal gyroscope (Fig. 2).

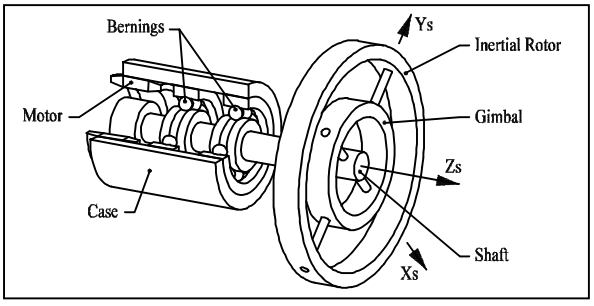

Figure 1 – DTG Configuration

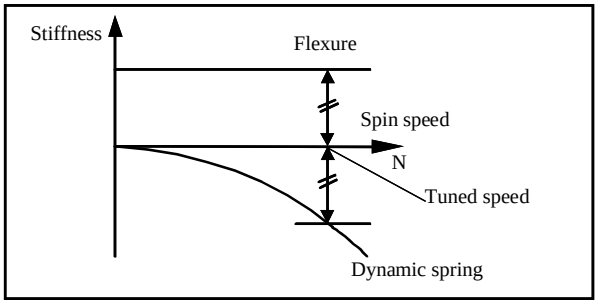

Figure 2 –The Tuning Speed

A complete mathematical model was derived by Craig (1973a, b), for a DTG composed by an arbitrary number of gimbals. Based on his work, a system of equations was derived for the usual DTG (one gimbal) by de Barros and Junqueira (2005), and presented, as in the IEEE handbook (IEEE, 1989), through equations (1) and (2).

The kinematic relations use four axis systems: (x_s, y_s, z_s) at the motor shaft, (x_g, y_g, z_g) at the gimbal, (x_r, y_r, z_r) at the rotor, and the cage system (x_c, y_c, z_c). They are illustrated in Figs. 3 and 4. Assuming small deflections, $\vec{\phi}$ is the absolute angular velocity of the cage, with components $\dot{\phi}_{xc}$ and $\dot{\phi}_{yc}$ in the cage system, and represent the input to the DTG model. The shaft speed relative to the cage is N.

The flexible joint is responsible for transmitting spring torques ($k \cdot \theta_{xc}$, $k \cdot \theta_{yc}$) and gyroscopic reactions ($N^2 \cdot J \cdot \theta_{xc}$, $N^2 \cdot J \cdot \theta_{yc}$), that cancel each other at the tuning speed. Other inertia moments transmitted by the joint are oscillating at a frequency, which is the double of the spin speed.

A drag moment T_d , between case and rotor, is proportional to the spin speed N . It acts on the motor axis direction (zs), and has components ($-Td \cdot \theta_y$) and ($Td \cdot \theta_x$) on the x_r and y_r respectively. There are also moments from the viscous damping, proportional to the relative angular speeds between case and rotor, $Dr \cdot \dot{\theta}_{xc}$ e $Dr \cdot \dot{\theta}_{yc}$, acting on directions x_c e y_c respectively.

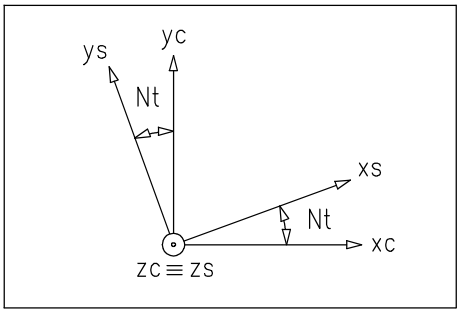

Figure 3. Relation between Cage and Shaft Axis.

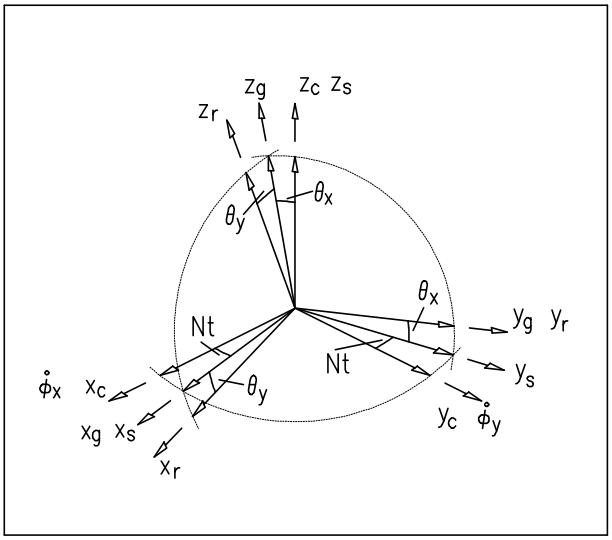

Figure 4. Rotor Angular Displacement.

A drag moment T_d , between case and rotor, is proportional to the spin speed N . It acts on the motor axis direction (zs), and has components ($-Td \cdot \theta_y$) and ($Td \cdot \theta_x$) on the x_r and y_r respectively. There are also moments from the viscous damping, proportional to the relative angular speeds between case and rotor, $Dr \cdot \dot{\theta}_{xc}$ e $Dr \cdot \dot{\theta}_{yc}$, acting on directions x_c e y_c respectively.

The torque coils apply moments, MC_x , MC_y , that are used in the control loops on the cage axes x_c e y_c , respectively. They make the rotor follow cage movements, and are proportional to the coil currents, that can be used also as measurements of the case angular displacement.

Considering the case motions as the inputs, the rotor dynamic equations based on the case fixed coordinates, assuming axi-symmetric gimbal, and rotor, are as follows:

$$\begin{aligned} &\ddot{\theta}_{xc} I + \dot{\theta}_{xc}(D + D_r) + \theta_{xc}(k - N^2 J) + \dot{\theta}_{yc} N(C + A_g) + \theta_{yc}\left(T_d + ND\right) \\ &= -\ddot{\phi}_x I - \dot{\phi}_y N(C + A_g - J) + MC_x - q_x \cos 2Nt - q_y sen2Nt \end{aligned} \tag{1}$$

$$\begin{aligned}&\ddot{\theta}_{yc}I + \dot{\theta}_{yc}(D + D_r) + \theta_{yc}(k - N^2 J) + \dot{\theta}_{xc}N(-C - A_g) - \theta_{xc}(T_D + DN)\\&= -\ddot{\phi}_y I + \dot{\phi}_x N(C + A_g - J) + MC_y - q_x sen2Nt + q_y \cos 2N\text{t}\end{aligned} \tag{2}$$

where,

C , C_g are the rotor, and gimbal z axis moments of inertia, respectively;

A , A_g are the rotor, and gimbal transverse axis moments of inertia, respectively;

$\dot{\theta}_{xc}$, $\dot{\theta}_{yc}$ are the rotor angular velocity along the case “x” and “y” axes;

$\dot{\phi}_{xc}$, $\dot{\phi}_{yc}$ are the absolute angular velocities of the gyroscope case, resolved along the case-fixed coordinate set.

$$I = \frac{1}{2}(2A + A_g)$$

$$J = \frac{1}{2}(2A_g - C_g)$$

$$q_x = \ddot{\theta}_{xc}\Delta I + \theta_{xc}N^2\Delta J + \dot{\theta}_{yc}N\Delta I + \theta_{yc} + \ddot{\phi}_x\Delta I - \dot{\phi}_y N(\Delta I + \Delta I_S)$$

$$q_y = \ddot{\theta}_{yc}\Delta I - \theta_{yc}N^2\Delta J - \dot{\theta}_{xc}2N\Delta I + \ddot{\phi}_y\Delta I - \dot{\phi}_x N(\Delta I + \Delta I_S)$$

$$\Delta I = \frac{1}{2}A_g$$

$$\Delta I_S = \frac{1}{2}(C_g - A_g)$$

$$\Delta J = \frac{1}{2}(C_g - 2A_g)$$

3 OPEN LOOP LINEAR MODEL

Assuming axi-symmetric rotor and gimbal, where gimbal inertias are much less than rotor inertias (Ag ,Cg << A, C), the coefficients included in qx e qy. can be neglected,, as well as the gimbal moment of inertia. The open loop (MCx= MCy=0) equations are then derived:

$$\ddot{\theta}_{xc}I + \dot{\theta}_{xc}(D + D_r) + \theta_{xc}(k - N^2 J) + \dot{\theta}_{yc}NC + \theta_{yc}(T_d + ND) = -\ddot{\phi}_x I - \dot{\phi}_y NC \tag{3}$$

$$\ddot{\theta}_{yc}I + \dot{\theta}_{yc}(D + D_r) + \theta_{yc}(k - N^2 J) - \dot{\theta}_{xc}NC - \theta_{xc}(T_d + ND) = -\ddot{\phi}_y I + \dot{\phi}_x NC \tag{4}$$

3.1 Ideal Condition

At the tuning condition, $N = N_0 = \sqrt{k/J}$, the joint torques are canceled by the gimbal reaction. In such case, without damping, the rotor would rotate free in the space, as expected from the ideal gyroscope. Beginning with aligned rotor and case axis, the equations above are further simplified to:

$$\theta_{xc}(t) = -\phi_x(t) \tag{5}$$

$$\theta_{yc}(t) = -\phi_y(t) \tag{6}$$

3.2 Open Loop Transfer Functions at Tuning Condition

The gyroscope time constant is an important parameter for evaluating the sensor quality. It is related to the damping effects acting upon the rotor. When turning the case around a transverse axis, such effects are responsible for aligning rotor and case, even without the torquer action. The rotor is, therefore, forced to a precession motion until its spin axis is coincident with the motor axis. The larger the time constant, the closer the sensor is to an ideal gyroscope.

Another typical motion present in the gyroscope is the rotor nutation, which produces oscillations in the sensor output.

Like in Craig (1972 b), the gyroscope transfer functions, derived from the former equations, can be represented in a way such that the dynamics of both phenomena are emphasized. Applying the Laplace Transform to (3) and (4), it follows:

$$P_1(s)\cdot\theta_{xc}(s)+P_2(s)\cdot\theta_{yc}(s)=-P_3(s)\cdot\phi_x(s)-P_4(s)\cdot\phi_y(s) \tag{7}$$

$$-P_2(s)\cdot\theta_{xc}(s)+P_1(s)\cdot\theta_{yc}(s)=P_4(s)\cdot\phi_x(s)-P_3(s)\cdot\phi_y(s) \tag{8}$$

The polynomials in “s” are defined by:

$$P_1(s)=I\cdot s^2+\left(D+D_r\right)\cdot s=Is[s+\frac{(D+D_r)}{I}]=Is(s+\frac{1}{\tau_1})$$

$$P_2(s)=N\cdot\left(C+A_g\right)\cdot s+\left(T_d+ND\right)=I\omega_n(s+\frac{1}{\tau})$$

$$P_3(s)=Is^2$$

$$P_4(s)=N\left(C+A_g-J\right)\cdot s=I\frac{N(C+A_g)}{I}s-\frac{(A_g+B_g-C_g)N}{2}s=I\omega_n s(1-\frac{1}{2Fm})$$

where,

$$\omega_n=\frac{\left(C+A_g\right)}{I}N$$

is the nutation frequency, and

$$\frac{1}{\tau_1}=\frac{D+Dr}{I}$$

$$\frac{1}{\tau}=\left(\frac{D}{I}+\frac{D_d}{I}\right)\frac{N}{\omega_n}$$

$$D_d=T_d\big/N$$

$$Fm=\frac{(C+A_g)}{(A_g+B_g-C_g)}$$

In matrix form, the relation between rotor and cage dynamics is:

$$\begin{bmatrix}\theta_{xc}(s)\\ \theta_{yc}(s)\end{bmatrix}=\begin{bmatrix}G_{11}(s) & G_{12}(s)\\ G_{21}(s) & G_{22}(s)\end{bmatrix}\cdot\begin{bmatrix}\phi_x(s)\\ \phi_y(s)\end{bmatrix} \tag{9}$$

where,

$$G_{11}(s)=G_{22}(s)=-\frac{P_1P_3+P_2P_4}{{P_1}^2+{P_2}^2}$$

$$G_{12}(s)=-G_{21}(s)=\frac{-P_1P_4+P_2P_3}{{P_1}^2+{P_2}^2}$$

These transfer functions are going to be re-arranged in a form where precession and nutation dynamics appear more explicitly. At first, the denominator is put as:

$$P_1^2(s)+P_2^2(s)=I^2[s^2(s+\frac{1}{\tau_1})^2+\omega_n^2(s+\frac{1}{\tau})^2] \tag{10}$$

Neglecting the other terns in s^2, when compared to ω_n^2, as well as $1/(\tau\cdot\tau_n)$ in the s coefficient, the former expression can be factorized in terms of the nutation and precession dynamics , as follows:

$$P_1^2(s)+P_2^2(s)=I^2[s^2(s+\frac{1}{\tau_1})^2+\omega_n^2(s+\frac{1}{\tau})^2]\cong I^2(s+\frac{1}{\tau_1})^2(s^2+\frac{2}{\tau_n}s+\omega_n^2) \tag{11}$$

where τ_n arises as the nutation time constant. Its value can be determined from the identity of terms in s^3:

$$\frac{1}{\tau_n}=\left(\frac{1}{\tau_1}-\frac{1}{\tau}\right)=\frac{D_r}{I}+\frac{D}{I}\left(1-\frac{N}{\omega_n}\right)-\frac{D_d}{I}\frac{N}{\omega_n} \tag{12}$$

The first two terms, in the right side of the above expression, act as dissipative terms for the nutation motion, since they represent damping for transversal motions between rotor and case. The last term represents the contribution originated from the drag moment T_d, whose effect is to attenuate the nutation damping, since it induces the rotor transversal motion when that is deflected by θ_x or θ_y, relative to the case.

The transfer function of the direct channel can also be simplified, by neglecting the term $1/(\tau\cdot\tau_n)$ in the numerator of G_{11}.

$$\begin{aligned}&P_1(s)P_3(s)+P_2(s)P_4(s)=I^2s\left\{s^2\left[\left(s+\frac{1}{\tau}\right)+\left(\frac{1}{\tau_1}-\frac{1}{\tau}\right)\right]+\omega_n^2\left(1-\frac{1}{2Fm}\right)\left(s+\frac{1}{\tau}\right)\right\}\\&\cong I^2s\left\{\left(s+\frac{1}{\tau}\right)\left[s^2+\frac{1}{\tau_n}s+\omega_n^2\left(1-\frac{1}{2Fm}\right)\right]\right\}\end{aligned} \tag{13}$$

Considering the typical relative orders of F_m and τ_1, the numerator of the cross channel can be approximated as follows:

$$P_2(s)P_3(s)-P_1(s)P_4(s)=I^2\omega_n s^2\left[\frac{1}{2Fm}s+\left(\frac{1}{\tau}-\frac{1}{\tau_1}\right)+\frac{1}{2\tau_1 Fm}\right]\cong I^2\omega_n s^2\left[\frac{1}{2Fm}s-\frac{1}{\tau_n}\right] \tag{14}$$

4. THE ROTOR PRECESSION

From the former results, a simple expression can be derived for representing the rotor precession. This can be seen after imposing a small deflection upon the rotor, relative to the cage, which can be represented by the step responses for G_{11} and G_{12}.

In order to extract easily the precession motion, it is assumed the pole-zero cancellation relative to the nutation dynamics in the direct channel (see equations 10 and 13). Therefore, G_{11} is given by:

$$G_{11}(s)=-\frac{s}{(s+\frac{1}{\tau})} \tag{15}$$

The step response of the cross channel can be neglect in this case. The output magnitude provided by G12 is negligible, as can be seen from the approximation:

$$G_{12}(s) = \frac{s^2[(\omega_n / 2Fm)s - (\omega_n / \tau_n)]}{(s+\frac{1}{\tau})^2(s^2 + \frac{2}{\tau_n}s + {\omega_n}^2)} \cong s^2[(1/2Fm\omega_n)s - (1/\omega_n\tau_n)]\left[\frac{1}{(s+\frac{1}{\tau})^2} - \frac{1}{(s^2 + \frac{2}{\tau_n}s + {\omega_n}^2)}\right] \tag{16}$$

Therefore, for step inputs with amplitudes $\phi_x(0)$, and $\phi_y(0)$ the response can be approximated by:

$$\theta_{xc}(t) = -\phi_x(0)e^{-t/\tau} \tag{17}$$

$$\theta_{yc}(t) = -\phi_y(0)e^{-t/\tau} \tag{18}$$

The expressions above show that rotor and case "*z axis*" agreement occurs at the time constant "τ". This parameter, as shown before, is a function of the drag moment acting along the rotor spin axis, and the damping for transverse motions between case and rotor.

The rotor precession, represented by expressions (17), and (18), can be explained by the analysis of the vector composition between drag and the DTG motor moments, as illustrated in Fig. 5. When the rotor is deflected in θ rad relative to the case, the drag moment component perpendicular to the spin axis, according to the gyroscopic effect, imposes a motion that aligns the rotor and case z-axes.

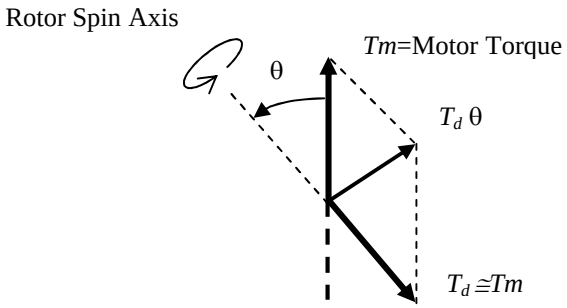

Figure 5. Drag torque producing the rotor precession.

5 EFFECT OF THE MISTUNED CONDITION

In practice, the DTG operates close to, but not exactly at the tuning condition. Inaccuracies at design and manufacturing, as well as changing characteristics along time, causes differences between the spin speed of the rotor, and the tuning frequency. The larger is the rate between rotor and gimbal inertia, the less is the spurious effect of the mistuning in the DTG performance. Such rate is expressed by the "figure of merit", *Fm* (Craig, 1973b). The influence of *Fm* is discussed in this section.

For small differences between the actual speed "*N*" and the tuning value "N_0", it follows:

$$(k - N^2 J) = J(N_0^2 - N^2) = J[(N + \delta N)^2 - N^2] = J(\delta N^2 + 2n\delta N) \tag{19}$$

Assuming $\delta N << N$, the next approximation is derived:

$$(k - N^2 J) \cong 2N\delta N = I\frac{(C + A_g)}{I}N\frac{\delta N}{(C + A_g)/2J} = I\omega_n\frac{\delta N}{Fm} \tag{20}$$

In such case, polynomial $P_1(s)$, and the numerator of $G_{12}(s)$ changes to:

$$P_1(s) = I[s^2 + (\frac{1}{\tau} + \frac{1}{\tau_n})s + \omega_n \frac{\delta N}{Fm}] \tag{21}$$

$$\begin{aligned} P_2(s)P_3(s) - P_1(s)P_4(s) &= I^2\omega_n s\left\{s\left(s+\frac{1}{\tau}\right) - \left[s^2 + \left(\frac{1}{\tau}+\frac{1}{\tau_n}\right)s + \omega_n\frac{\delta N}{Fm}\right]\left(1-\frac{1}{2Fm}\right)\right\} \\ &\cong I^2\omega_n s\left\{\frac{1}{2Fm}s^2 - \frac{1}{\tau_n}s - \omega_n\frac{\delta N}{Fm}\right\} \end{aligned} \tag{22}$$

Assuming that $\frac{\delta N}{Fm} << \omega_n$, the expression for the numerator of G_{11} can be considered as in (13), and the denominator of both transfer functions changes to:

$$P_1^2(s) + P_2^2(s) = I^2[(s+\frac{1}{\tau})^2 + \left(\frac{\delta N}{Fm}\right)^2](s^2 + \frac{2}{\tau_n}s + \omega_n^2) \tag{23}$$

Therefore, the new expressions for G_{11} and G_{12} are given by:

$$G_{11}(s) = \frac{s\left(s+\frac{1}{\tau}\right)\left[s^2 + \frac{1}{\tau_n}s + \omega_n^2\left(1-\frac{1}{2Fm}\right)\right]}{[(s+\frac{1}{\tau})^2 + \left(\frac{\delta N}{Fm}\right)^2](s^2 + \frac{2}{\tau_n}s + \omega_n^2)} \tag{24}$$

$$G_{12}(s) = \frac{\omega_n s\left\{\frac{1}{2Fm}s^2 - \frac{1}{\tau_n}s - \omega_n\frac{\delta N}{Fm}\right\}}{[(s+\frac{1}{\tau})^2 + \left(\frac{\delta N}{Fm}\right)^2](s^2 + \frac{2}{\tau_n}s + \omega_n^2)} \tag{25}$$

For the step response, a similar result to that presented by Craig can be obtained after some simplification in the transfer functions (24) and (25). Partial fraction decomposition of G12(s), fed by the inputs $\frac{\phi_x(0)}{s}$, $\frac{\phi_y(0)}{s}$, show that the contribution of the terms at the nutation and $\frac{\delta N}{Fm}$ frequencies can be neglected. Moreover, the pole-zero cancellation is assumed at the nutation dynamics. The simplified form of the transfer functions for calculating the step response is then given by:

$$G_{11}(s) = -\frac{s(s+\frac{1}{\tau})}{[(s+\frac{1}{\tau})^2 + \left(\frac{\delta N}{Fm}\right)^2]} \tag{26}$$

$$G_{12}(s) = \frac{-s(\delta N / Fm)}{[(s+\frac{1}{\tau})^2 + \left(\frac{\delta N}{Fm}\right)^2]} \tag{27}$$

The response is in the time domain is:

$$\theta_{xc}(t) = -\phi_x(0)e^{-t/\tau}\cos(\frac{\delta N}{Fm})\,t - \phi_y(0)e^{-t/\tau}sen(\frac{\delta N}{Fm})t \tag{28}$$

$$\theta_{yc}(t) = \phi_x(0)e^{-t/\tau}\, sen(\frac{\delta N}{Fm})t - \phi_y(0)e^{-t/\tau}\cos(\frac{\delta N}{Fm})t \tag{29}$$

Figure 6 shows the precession simulation according to different models presented so far: the original, non-linear model (eqs. 1, and 2), the linear model from eqs.3 and 4, and the response generated by expressions (28) and (29), that are originated from the simplified transfer functions G_{11} and G_{12} in (26), and (27). The particulars of the DTG are presented in table 1. Results show the good agreement among the responses generated by those models, validating the approximations.

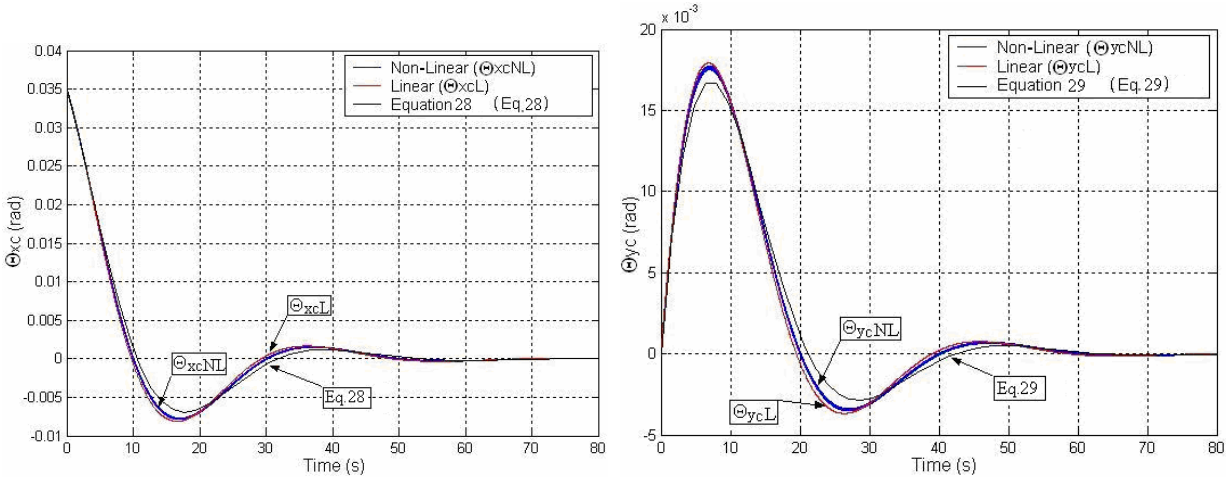

(a) **(b)**

Figure 6. Rotor Precession at Mistuning Condition. (a): direct axis; (b): cross axis

6. MODELING OF THE CONTROL SYSTEM COMPONENTS

The DTG control system provides the rotor tracking to the case motions as well as the measurement of the motion angular rate.The plant is represented by the rotor, and two control loops are formed by the electronics for the direct channel and for the inverse channel (Fig.7). The main components of the electronic circuit are represented in Fig. 8

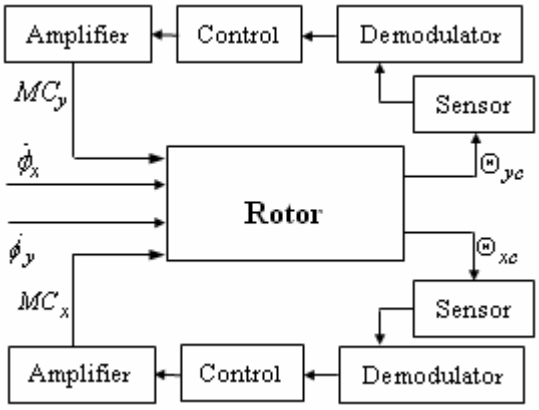

Figure 7. Control System Main Modules

The oscillator excites the four pick-off (2 for each axis) primary coils. The output voltage generated at the coils excites the demodulator. At this stage, the signal is rectified, filtered and added to the signal from the other pick-off

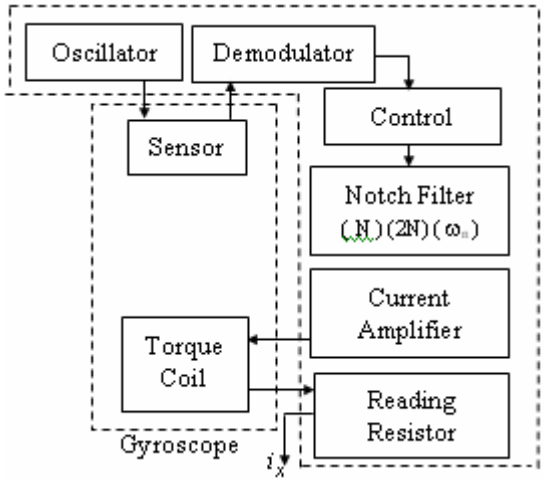

Figure 8. Main Components of the Control System Electronics

6.1 Pickoff and Demodulator Module

Variable reluctance transformers are used for representing the pickoffs. The primary coil is excited by an oscillator, and the secondary coil is connected to a demodulator. The output voltage from the secondary coil is modulated as a consequence of the effect from the variable gap between the rotor and the pickoff transformers (Fig. 10).

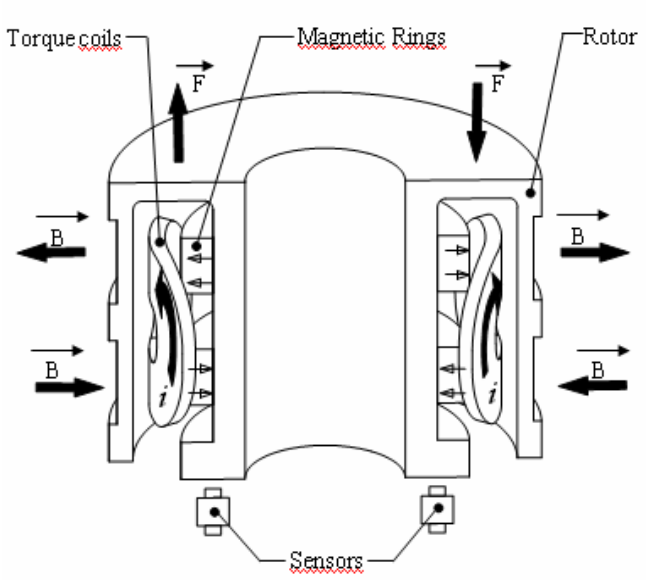

Figure 9. Elements of the DTG control system: pick-off, and torque coils

The demodulator is fed by the outputs from a pair of pickoffs. The signals are rectified at opposite phases, and summed up. The output is then filtered in order to cut-off frequencies above the pickoff fundamental frequency and to eliminate the DC bias. The circuit is designed so that the whole module works as a constant gain in the interest frequency range.

6.2 Controller

The signal generated at the demodulator may include noise, having peaks at frequencies N (the motor speed), 2N (from the perturbations generated at the gimbal), and at the nutation frequency. Therefore, the first stage of the controller module is composed by a series of filters at those characteristic frequencies. The next phase is responsible for cutting off the bias, the high frequency perturbations, and stabilizing the system. A kind of lead-lag circuit can cope with such task.

6.3 Current Regulator

The signal from the controller is transformed in a control current to be fed into the torque coils. A current regulator can be implemented by a feedback amplifier (Fig. 10).

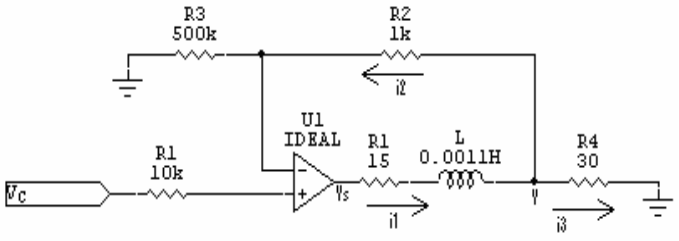

Figure 10. Current Regulator

7. CONCLUSIONS

Compared to the classical works of Craig (1972 a, b) , a clearer and improved approach for deriving the mathematical model was proposed for a single gimbal dynamically tuned gyroscope. All equations for linear, and non-linear models were implemented numerically in Matlab. Future steps for this investigation include the use of simulator for testing the DTG performance sensitivity to parameter variation, such as the figure of merit, damping constants, etc. Moreover, the simulator will be employed for investigating different strategies for filtering and controller design.

ACKNOWLEDGEMENT

This work has been supported by the Brazilian Space Agency. The second author was sponsored by the Fapesp foundation through a scholarship.

REFERENCES

Craig, R. J. G. Theory of Operation of an Elastically Supported, Tuned Gyroscope, IEEE Trans. on Aerospace and Electronic Systems, pp. 280-288. vol AES-8, No 3, 1972a.

Craig, R. J. G. Theory of Errors of a Multigimbal, Elastically Supported, Tuned Gyroscope, IEEE Trans. on Aerospace and Electronic Systems, pp. 289-297. vol AES-8, No 3, 1972b.

Craig, R. J. G. Dynamically Tuned Gyros in Strapdown Systems. AGARD Conference on Inertial Navigation Computers and Systems. Firenze, Italy. pp. 12-1 to 12-17. 1972c.

de Barros, E. A., F. C. Junqueira. Modelagem Matemática de um Giroscópio Sintonizado Dinamicamente. Revista Controle e Automação. Vol. 16. No. 2. 2005.

Haberland, 1978. Technical Advances through a Novel Gyro Hinge Design. DGCON Symposium ueber Kreiseltech. Duesseldorf. Germany. Sept. 1978.

Howe, E. W., Savet, P. H. The Dynamically Tuned Free Rotor Gyro. Control Engineering. pp. 67-72. June. 1964.

IEEE – Std 813-1988. Specification Format Guide and Test Procedure for Two-Degree-of Freedom, Dynamically Tuned Gyros. IEEE, 1989, New York. USA.

Joos, D. K. Comparison of Typical Gyro Errors for Strapdown Applications. DGCON Symposium Gyro Technology, Stuttgart, Germany, 1977.

Karnick, H. Experience based upon Experimental Dry Tuned Gyros. DGON Symposium Gyro Technology, Stuttgart, Germany, 1979.

Lawrence, A. Modern Inertial Navigation: Navigation Guidance, and Control. Second Edition. Springer. New York. 1998. (Mechanical Engineering Series).

Mansour, W. M., Lacchini, C. Two-Axis Dry Tuned-Rotor Gyroscope Design and Technology. Journal of Guidance, Control and Dynamics. Vol 16, No 3, Maio-Junho 1993.

RESPONSIBILITY NOTICE

The authors are the only responsible for the printed material included in this paper.